

Charging Dynamics of Overlapping Double Layers in a Cylindrical Nanopore

Ankur Gupta^{1,†}, Pawel J. Zuk^{1,2,‡} and Howard A. Stone^{1,*}

¹*Department of Mechanical and Aerospace Engineering, Princeton University, Princeton, New Jersey 08544, USA*

²*Institute of Fundamental Technological Research, Polish Academy of Sciences, Pawińskiego 5b, 02-106 Warsaw, Poland*

 (Received 26 March 2020; revised 3 May 2020; accepted 10 July 2020; published 11 August 2020)

The charging of electrical double layers inside a cylindrical pore has applications to supercapacitors, batteries, desalination and biosensors. The charging dynamics in the limit of thin double layers, i.e., when the double layer thickness is much smaller than the pore radius, is commonly described using an effective RC transmission line circuit. Here, we perform direct numerical simulations (DNS) of the Poisson-Nernst-Planck equations to study the double layer charging for the scenario of overlapping double layers, i.e., when the double layer thickness is comparable to the pore radius. We develop an analytical model that accurately predicts the results of DNS. Also, we construct a modified effective circuit for the overlapping double layer limit, and find that the modified circuit is identical to the RC transmission line but with different values and physical interpretation of the capacitive and resistive elements. In particular, the effective surface potential is reduced, the capacitor represents a volumetric current source, and the charging timescale is weakly dependent on the ratio of the pore radius and the double layer thickness.

DOI: 10.1103/PhysRevLett.125.076001

Porous electrodes with pore diameters between 0.5–10 nm range are commonly utilized in supercapacitors [1,2], batteries [3,4], desalination [5] and biosensors [6]. These pores are filled with ions that are attracted to the surface of the pore and form an electrical double layer. The charging dynamics of such a system is typically modeled as an RC transmission line, first proposed by de Levie [7], where the double layers (DLs) are represented as capacitive elements and the electroneutral solution is represented by a resistive element. Over the past three decades, numerous studies have been conducted that exploit some form of the RC transmission line model to understand the self-discharge mechanism [8–10], the effect of pore size and shape [11–18], and the effect of electrolyte concentration [19,20], among others [21]. More recently, several studies have argued for more detailed analysis of ion transport inside the DL [4,5,22–26].

The ratio of DL thickness to the pore radius impacts the ion transport inside a cylindrical pore [4,5,7,26]. The standard RC transmission line model assumes that the DL thickness is significantly smaller than the pore radius [7]. However, since the concentrated electrolytes can behave as dilute electrolytes [27] with DL thickness as large as 5–10 nm [27–29], and since the typical pore radii in experiments are between 0.5–10 nm [1,2], the DL thickness

is often comparable to the pore size. Some reports have acknowledged the limit of the RC transmission model [4,5,30] but a model of the charging dynamics that describes the overlapping DL limit remains unavailable. In this Letter, we overcome these limitations by performing direct numerical solutions (DNS) on the Poisson-Nernst-Planck (PNP) equations. In addition, we introduce a reduced-order model that quantitatively agrees with the results from DNS and is applicable to the scenario of overlapping DLs. Specifically, we study the overlapping DL limit for small potentials and dilute electrolyte concentrations, i.e., the physical conditions when the PNP equations are valid.

We consider a cylindrical pore of radius a and length ℓ_{pore} where $a/\ell_{\text{pore}} \ll 1$. The pore is filled with a binary electrolyte such that the cation and anion valences are equal to unity [Fig. 1(a)]. We assume that the pore wall exhibits an ideal blocking electrode condition, i.e., the normal flux of ions vanishes at the pore wall. We further assume that the diffusivities of the ions are equal and are denoted by \mathcal{D} . We describe the cation and anion concentrations by variables $c_{\pm}(r, z, t)$ and the electrical potential by $\psi(r, z, t)$, where r is the radial direction, z is the axial direction, and t is time. The mouth of the pore is at $z = 0$. In addition, we assume that there exists a stagnant diffusion layer (SDL) of thickness ℓ_{SDL} and cross sectional area A_{SDL} . The bulk is located at $z = -\ell_{\text{SDL}}$ where $c_{\pm} = c_0$ and $\psi = 0$ [Fig. 1(a)]. In the uncharged state, i.e., $t < 0$, the system is electroneutral everywhere. At $t = 0$, the walls of the pore are set to a constant potential ψ_D such that the counterions are attracted towards the pore wall to form a DL in the radial direction. During the charging process, i.e., $t > 0$, the charge inside the DL begins to accumulate such that the charge decreases

Published by the American Physical Society under the terms of the [Creative Commons Attribution 4.0 International license](https://creativecommons.org/licenses/by/4.0/). Further distribution of this work must maintain attribution to the author(s) and the published article's title, journal citation, and DOI.

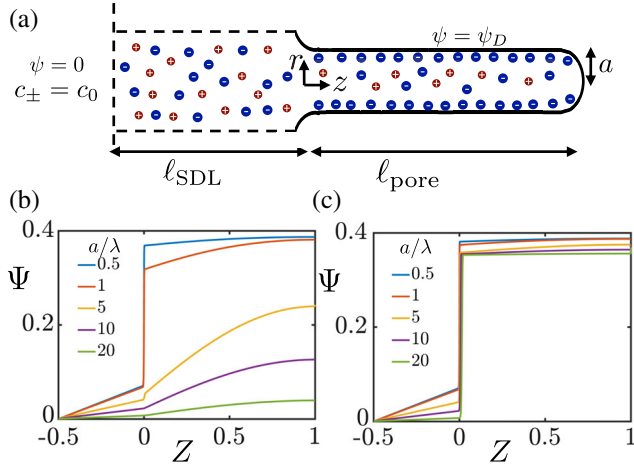


FIG. 1. Problem setup and results from DNS. (a) A cylindrical pore of radius a and length ℓ_{pore} with an applied potential ψ_D . The pore interacts with the bulk through a stagnant diffusion layer with thickness ℓ_{SDL} and cross sectional area A_{SDL} . (b) Plot of dimensionless potential $\Psi(R=0, Z, \tau=0.14)$ at the center of the geometry for different a/λ . (c) Plot of dimensionless potential $\Psi(R \rightarrow 1, Z, \tau=0.14)$ near the surface of the pore for different a/λ . Plots are presented for $\Psi_D = 0.4$, $\lambda/\ell_{\text{pore}} = 10^{-3}$, $A_{\text{SDL}}/(\pi a^2) = 4$ and $\ell_{\text{SDL}}/\ell_{\text{pore}} \approx 0.5$.

along the length of the pore. In the fully charged state, the axial gradients vanish and the charge stored inside the DL is constant throughout the length of the pore.

We define dimensionless charge density $\rho = (c_+ - c_-)/c_0$, salt concentration $s = (c_+ + c_-)/c_0$, time $\tau = tD/\ell_{\text{pore}}^2$ and potential $\Psi = e\psi/(k_B T)$. The coupled PNP equations can thus be written as

$$\frac{\partial \rho}{\partial \tau} = \nabla^2 \rho + \nabla \cdot (s \nabla \Psi), \quad (1a)$$

$$\frac{\partial s}{\partial \tau} = \nabla^2 s + \nabla \cdot (\rho \nabla \Psi), \quad (1b)$$

$$-\left(\frac{\lambda}{\ell_{\text{pore}}}\right)^2 \nabla^2 \Psi = \frac{\rho}{2}, \quad (1c)$$

where the dimensionless coordinates are $Z = z/\ell_{\text{pore}}$, $R = r/a$, $\nabla = (\ell_{\text{pore}}/a)\mathbf{e}_r(\partial/\partial R) + \mathbf{e}_z(\partial/\partial Z)$, $\lambda = \sqrt{\epsilon k_B T / (2e^2 c_0)}$ is the Debye length, ϵ is the electrical permittivity, k_B is the Boltzmann constant, T is the temperature and e is the charge on an electron. We perform DNS using OpenFOAM [31]. We set $\Psi_D = 0.4$, $\lambda/\ell_{\text{pore}} = 10^{-3}$, $A_{\text{SDL}}/(\pi a^2) = 4$, $\ell_{\text{SDL}}/\ell_{\text{pore}} \approx 0.5$, $0.5 \leq a/\lambda \leq 20$, and solve the system of Eqs. (1) [31]. The boundary condition for Ψ are (i) $\Psi = \Psi_D$ at the pore walls, (ii) $\Psi = 0$ in the reservoir, and (iii) zero normal gradient of potential at the boundaries of the SDL. The boundary condition for ρ and s are (i) zero normal flux at the

pore walls, (ii) $\rho = 0$ and $s = 2$ at the reservoir, and (iii) zero normal flux at the boundaries of the SDL. The initial conditions are $\rho = 0$ and $s = 2$ everywhere with Ψ satisfying Laplace's equation with the aforementioned boundary conditions (see [31] for details).

The results from DNS indicate that the variation in potential at the center of the geometry $\Psi(0, Z, \tau)$ with Z depends significantly on a/λ ; see Fig. 1(b). For the thin DL scenario, i.e., $a/\lambda \gg 1$, the potential varies gradually across the $Z = 0$ interface. However, for the overlapping DLs, i.e., $a/\lambda \leq 1$, the potential changes rapidly across $Z = 0$. In contrast, the potential near the surface of the pore $\Psi(R \rightarrow 1, Z, \tau)$ increases rapidly across $Z = 0$ for all a/λ ; see Fig. 1(c). These trends suggest that the potential rapidly increases due to the presence of the electrical DL. For the thin DL, the DL is present only close to the surface and thus the rapid increase in potential across $Z = 0$ is observed only near $R \rightarrow 1$. On the other hand, for overlapping DLs, the DL is present throughout the pore cross section and the potential increases rapidly across $Z = 0$ for all R .

Next, we focus on a reduced-order model inside the pore, i.e., $0 < Z \leq 1$, for the overlapping DLs scenario. In this limit, we cannot invoke electroneutrality inside the pore. Furthermore, we can not exploit the separation of length scales. However, in the linear limit $\Psi_D \ll 1$, we can assume that the salt concentration is constant everywhere and for all times, i.e., $s = 2$ [31]. This observation eliminates the need to solve Eq. (1b). Moreover, since the radial flux of ρ at $R = 0$ and $R = 1$ vanishes, we assume the radial flux of ρ vanishes for all R . Therefore, we obtain

$$\frac{\partial \rho}{\partial R} + 2 \frac{\partial \Psi}{\partial R} = 0, \quad (2)$$

or

$$\rho(R, Z, \tau) - \rho_m(Z, \tau) = -2(\Psi(R, Z, \tau) - \Psi_m(Z, \tau)), \quad (3)$$

where $\rho_m(Z, \tau)$ and $\Psi_m(Z, \tau)$ are, respectively, the centerline charge and potential, which are to be determined. We substitute Eq. (3) into Eq. (1c). Next, we assume that $\partial^2/\partial Z^2 \ll (\ell_{\text{pore}}/a)^2 \partial^2/\partial R^2$, and integrate with boundary conditions $\partial \Psi/\partial R|_{R=0} = 0$ and $\Psi(1, Z, \tau) = \Psi_D$ to obtain

$$\frac{\Psi - \Psi_m - \rho_m/2}{\Psi_D - \Psi_m - \rho_m/2} = \frac{I_0(R\frac{a}{\lambda})}{I_0(\frac{a}{\lambda})}, \quad (4)$$

where I_n is the modified Bessel function of the first kind of order n . We note that as $Z \rightarrow 1$, Eq. (4) does not capture the effects of a change in geometry. However, since $a/\ell_{\text{pore}} \ll 1$, we can neglect the end effects. Using $\Psi = \Psi_m$ at $R = 0$ in Eq. (4) yields a relation between centerline charge and potential:

$$\rho_m = \frac{2(\Psi_m - \Psi_D)}{I_0\left(\frac{a}{\lambda}\right) - 1}. \quad (5)$$

Substituting Eq. (5) in (3) and (4), it is straightforward to show

$$\frac{\rho}{\rho_m} = I_0\left(R\frac{a}{\lambda}\right). \quad (6)$$

Finally, we substitute $s = 2$ and Eq. (5) in (1), and evaluate at the center of the pore, to arrive at

$$\frac{\partial \Psi_m}{\partial \tau} = I_0\left(\frac{a}{\lambda}\right) \frac{\partial^2 \Psi_m}{\partial Z^2}, \quad (7)$$

which is the governing equation for the centerline potential distribution inside the pore for overlapping DLs. Equation (7) suggests a charging timescale $t_{c,\text{overlap}} = \ell_{\text{pore}}^2 / (I_0(a/\lambda)D)$, which is quite different from the corresponding thin DL limit, as we show later. The initial condition is $\Psi_m(Z, 0) = \Psi_D$. The boundary condition at the end of the pore $Z = 1$ is simply $\partial \Psi_m / \partial Z = 0$. Next, we focus on the boundary condition at $Z = 0$ where the pore contacts the SDL.

We assume that the SDL is electroneutral ($\rho = 0$), which yields a linear variation in Ψ_m for $Z \leq 0$; see Eq. (1c). In addition, we treat the sudden increase in the potential across $Z = 0$ [Fig. 1(b)] as a discontinuity. To this end, we define $\Psi_1 = \Psi_m(0, 0^-, \tau)$, i.e., the potential just outside the mouth of the pore, and $\Psi_2 = \Psi_m(0, 0^+, \tau)$, i.e., the potential just inside the mouth of the pore. Similarly, we define $\rho_1 = \rho_m(0, 0^-, \tau) = 0$ and $\rho_2 = \rho_m(0, 0^+, \tau)$. We equate the current from the SDL with the current inside the pore at $Z = 0$ to obtain

$$\left. \frac{\partial \Psi_2}{\partial Z} \right|_{0^+} = \frac{A_{\text{SDL}}}{\pi a^2} \left(\frac{I_0\left(\frac{a}{\lambda}\right) - 1}{I_0\left(\frac{a}{\lambda}\right)} \right) \left(\frac{a/\lambda}{2I_1\left(\frac{a}{\lambda}\right)} \right) \left. \frac{\partial \Psi_1}{\partial Z} \right|_{0^-}, \quad (8)$$

where $\partial \Psi_1 / \partial Z = (\Psi_1 / \ell_{\text{SDL}}) \ell_{\text{pore}}$ (recall that Ψ_m is linear in SDL due to electroneutrality). To relate Ψ_1 and Ψ_2 , we invoke the condition that the charge flux in the transition region is equal to the charge flux in the diffusion layer, or

$$\frac{\rho_2 - \rho_1}{\delta Z} + 2 \frac{\Psi_2 - \Psi_1}{\delta Z} = 2 \frac{\Psi_1}{\ell_{\text{SDL}}}, \quad (9)$$

where δZ is the thickness of the thin transition region. Since $\delta Z / \ell_{\text{SDL}} \ll 1$, we get the condition $\rho_2 - \rho_1 = 2(\Psi_1 - \Psi_2)$. Physically, this implies that the charge fluxes arising from the diffusion and electromigration in the transition region balance each other to maintain current equality. By substituting $\rho_1 = 0$ and $\rho_2 = (\Psi_2 - \Psi_D) / (I_0(a/\lambda) - 1)$ [from Eq. (5)] in the aforementioned condition, we get

$$\Psi_1 = \frac{\Psi_2 I_0\left(\frac{a}{\lambda}\right) - \Psi_D}{I_0\left(\frac{a}{\lambda}\right) - 1}. \quad (10)$$

By utilizing Eq. (10) in (8), we obtain

$$\frac{\partial \Psi_2}{\partial Z} = \text{Bi} \left(\Psi_2 - \frac{\Psi_D}{I_0\left(\frac{a}{\lambda}\right)} \right), \quad (11)$$

where

$$\text{Bi} = \frac{a/\lambda}{2I_1\left(\frac{a}{\lambda}\right)} \frac{\ell_{\text{pore}} A_{\text{SDL}}}{\ell_{\text{SDL}} \pi a^2}. \quad (12)$$

By a further change of variables $\phi = \Psi_m - \Psi_D / I_0(a/\lambda)$ and $T = \tau I_0(a/\lambda)$, we can rewrite Eqs. (7) and (11) as

$$\frac{\partial \phi}{\partial T} = \frac{\partial^2 \phi}{\partial Z^2}, \quad (13)$$

which is to be solved with boundary conditions $\partial \phi / \partial Z = \text{Bi} \phi$ at $Z = 0$ and $\partial \phi / \partial Z = 0$ at $Z = 1$. The analytical solution to this equation is

$$\phi = \phi_D \sum_{n=0}^{\infty} \frac{4 \sin \lambda_n}{2\lambda_n + \sin 2\lambda_n} \exp(-\lambda_n^2 T) \cos[\lambda_n(Z - 1)], \quad (14)$$

where $\lambda_n \tan \lambda_n = \text{Bi}$ and $\phi_D = \Psi_D (I_0(a/\lambda) - 1) / I_0(a/\lambda)$. Equation (14) provides a solution for the centerline potential $\Psi_m(Z, \tau)$ and Eqs. (4)–(6) can subsequently be used to predict $\rho_m(Z, \tau)$, $\rho(R, Z, \tau)$, and $\Psi(R, Z, \tau)$ for the overlapping DL limit.

We briefly summarize the “RC transmission line” model for the thin DL limit [5,7]. This model assumes that the region outside the DL is electroneutral ($\rho = 0$) and can be represented by an effective resistance per unit length $\mathcal{R}_{\text{pore}}$; see Fig. 2. Consequently, the potential outside the DL is only dependent on the axial direction. The DLs are represented through an effective capacitance per unit (axial) length $\mathcal{C}_{\text{pore}}$ such that the current from the capacitors in the radial direction is transported through the resistors in the axial direction; see Fig. 2. Finally, the SDL is assumed to be electroneutral and is thus also represented by an effective resistance per unit length \mathcal{R}_{SDL} . For the linear limit $\Psi_D \ll 1$, $\mathcal{C}_{\text{pore}} = 2\pi a \epsilon / \lambda$, $\mathcal{R}_{\text{pore}} = \lambda^2 / (\pi a^2 D \epsilon)$ and $\mathcal{R}_{\text{SDL}} = \lambda^2 / (A_{\text{SDL}} D \epsilon)$. Inside the pore, the current at an arbitrary location z can be evaluated as $i(z) = \mathcal{R}_{\text{pore}}^{-1} \partial \psi / \partial z$.

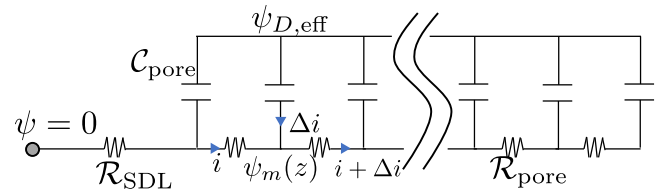


FIG. 2. Effective circuit model is identical for the thin and overlapping DL limits. However, the values of $\mathcal{C}_{\text{pore}}$, $\mathcal{R}_{\text{pore}}$, \mathcal{R}_{SDL} , and $\psi_{D,\text{eff}}$ are different for the two limits. A summary of these values is provided in Table I.

TABLE I. Summary of parameters for the effective circuit models in the limits of thin and overlapping DL as shown in Fig. 2. The values of resistance and capacitance are described per unit axial length.

	thin DL	overlapping DL
C_{pore}	$(\varepsilon/\lambda)2\pi a$	$(\varepsilon/\lambda^2)\pi a^2$
$\mathcal{R}_{\text{pore}}$	$\lambda^2/(\pi a^2 \mathcal{D} \varepsilon)$	$\lambda^2/(\pi a^2 \mathcal{D} \varepsilon I_0(a/\lambda))$
\mathcal{R}_{SDL}	$\lambda^2/(A_{\text{SDL}} \mathcal{D} \varepsilon)$	$2\lambda^3 I_1(a/\lambda)/(a A_{\text{SDL}} \mathcal{D} \varepsilon I_0(a/\lambda))$
$\psi_{D,\text{eff}}$	ψ_D	$\psi_D(I_0(a/\lambda) - 1)/I_0(a/\lambda)$
t_c	$(2\lambda/a)\ell_{\text{pore}}^2/\mathcal{D}$	$\ell_{\text{pore}}^2/(I_0(a/\lambda)\mathcal{D})$

Furthermore, the change in axial current is equal to the current arising from the capacitor, or $\partial i/\partial z = C_{\text{pore}}\partial\psi/\partial t$. In dimensionless units, we get [5,7]

$$\frac{\partial\Psi}{\partial\tilde{\tau}} = \frac{\partial^2\Psi}{\partial Z^2}, \quad (15)$$

where $\tilde{\tau} = \tau(a/2\lambda)$, $\Psi(Z, 0) = \psi_D$ is the initial condition, and the boundary conditions are $\partial\Psi/\partial Z = 0$ at $Z = 1$, and $\partial\Psi/\partial Z = \text{Bi}\Psi$ at $Z = 0$, where $\text{Bi} = \ell_{\text{pore}}\mathcal{R}_{\text{pore}}/(\ell_{\text{SDL}}\mathcal{R}_{\text{SDL}}) = \ell_{\text{pore}}A_{\text{SDL}}/(\ell_{\text{SDL}}\pi a^2)$. The RC transmission model suggests that the timescale of charging $t_{c,\text{thin}} = \mathcal{R}_{\text{pore}}C_{\text{pore}}\ell_{\text{pore}}^2 = (2\lambda/a)\ell_{\text{pore}}^2/\mathcal{D}$ [37]. We highlight that $t_{c,\text{thin}}$ varies inversely with a/λ whereas for the overlapping DL limit $t_{c,\text{overlap}} = \ell_{\text{pore}}^2/(I_0(a/\lambda)\mathcal{D})$, is weakly dependent on a/λ .

We note that the mathematical structure of the governing equations in the two limits of DL thickness, i.e., Eqs. (13) and (15), is identical. Therefore, the effective circuit model for the overlapping DLs remains the same; see Fig. 2. However, the values of capacitance, resistances and the effective wall potential are $C_{\text{pore}} = (\varepsilon/\lambda^2)\pi a^2$, $\mathcal{R}_{\text{pore}} = \lambda^2/(\pi a^2 \mathcal{D} \varepsilon I_0(a/\lambda))$, $\mathcal{R}_{\text{SDL}} = 2\lambda^3 I_1(a/\lambda)/(a A_{\text{SDL}} \mathcal{D} \varepsilon I_0(a/\lambda))$, and $\psi_{D,\text{eff}} = \psi_D(I_0(a/\lambda) - 1)/I_0(a/\lambda)$; see Fig. 2 and Table I.

Physically, three key features differentiate the scenario of the overlapping DLs ($a/\lambda \lesssim 1$) from the thin DLs ($a/\lambda \gg 1$). First, the effective driving force for DL charging is reduced from ψ_D to $\psi_{D,\text{eff}} = \psi_D(I_0(a/\lambda) - 1)/I_0(a/\lambda)$. Second, since the DLs fill the entire pore, the capacitor represents a volumetric current source (see C_{pore} in Table I), which is in contrast to the thin DL limit where the capacitor is a surface areal current source. Lastly, the effective resistance from the static diffusion layer is different as compared to the thin DL limit as this resistance also depends on the geometric parameter a/λ ; see Table I. Overall, due to the reduced $\psi_{D,\text{eff}}$, the net current predicted from the overlapping DL model would be lower than the current predicted by extrapolating the thin DL limit. Furthermore, due to the volumetric nature of capacitance, the effective time scale of

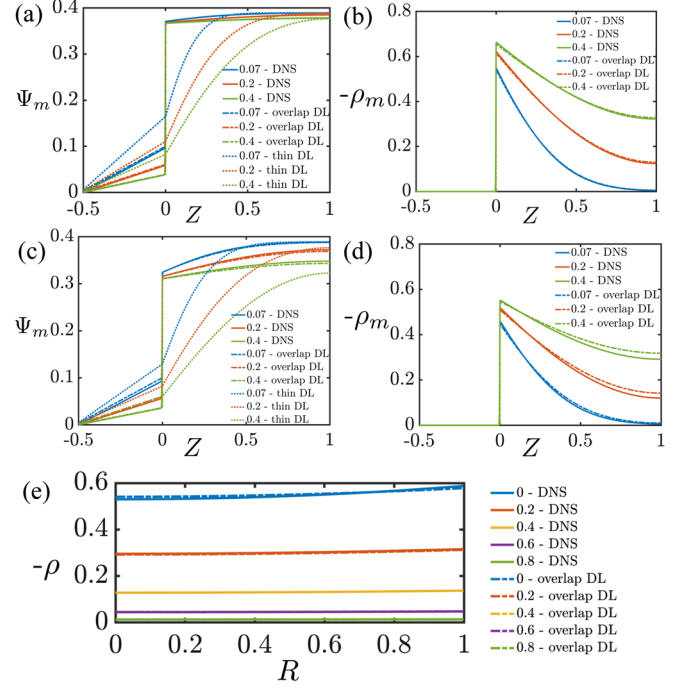


FIG. 3. Comparison of effective circuit models with the results from DNS. (a) Potential at the center of the pore $\Psi_m(Z, \tau = 0.07, 0.2, 0.4)$ and (b) local charge at the center of the pore $\rho_m(Z, \tau = 0.07, 0.2, 0.4)$ for $a/\lambda = 0.5$. (c) $\Psi_m(Z, \tau = 0.07, 0.2, 0.4)$ and (d) $\rho_m(Z, \tau = 0.07, 0.2, 0.4)$ for $a/\lambda = 1$. (e) Radial variation of charge $\rho(R, Z, \tau)$ for $Z = 0, 0.2, 0.4, 0.6, 0.8$ and $\tau = 0.07$ for $a/\lambda = 0.5$.

charging becomes the diffusion time scale along the pore, or $t_{c,\text{overlap}} \approx \ell_{\text{pore}}^2/\mathcal{D}$.

Next, we compare the predictions of the reduced-order models with the results from the DNS simulation for $a/\lambda = 0.5$ and $a/\lambda = 1$ [Fig. 3]. The overlapping DL model displays excellent agreement between $\Psi_m(Z, \tau)$ and the DNS simulations, including the rapid increase in Ψ_m across $Z = 0$; see Figs. 3(a) and 3(c). We note that the thin DL model is unable to capture the variation in Ψ_m and thus should not be extrapolated in systems where $a/\lambda \lesssim O(1)$. Furthermore, the predicted $\rho_m(Z, \tau)$ also exhibits excellent quantitative agreement with the DNS results; see Figs. 3(b) and 3(d). Lastly, our model is able to capture the radial variation in $\rho(R, Z, \tau)$; see Fig. 3(e). Therefore, our model is able to capture most of the details of the DNS solution.

We plot the dimensionless current at the mouth of the pore $I(\tau)$, i.e., current normalized by $\pi a^2 \varepsilon c_0 \mathcal{D} / \ell_{\text{pore}}$, for different a/λ [Fig. 4]. We find that $I(\tau)$ decreases with an increase in a/λ , which implies that the utilization of pore volume for DL charging decreases with an increase in a/λ . We observe that the thin DL model is able to accurately predict $I(\tau)$ for $a/\lambda = 5$ and 20 [Fig. 4]. However, for $a/\lambda = 0.5$, the predicted values of $I(\tau)$ from the thin DL model are significantly higher than those predicted by the DNS simulations. In contrast, our overlapping DL model is

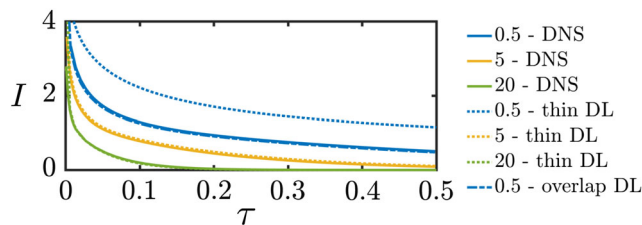


FIG. 4. Dimensionless current $I(\tau)$ at the mouth of the pore for different a/λ . The predictions from the thin DL and overlapping DL models are also provided.

able to quantitatively capture the trend. The reduction in the values of $I(\tau)$ between the two models arises mainly because of the lower $\Psi_{D,\text{eff}}$, an important feature not captured by the thin DL model.

The analytical form of our analysis can be readily used to characterize cyclic voltammetry data in experimental investigations of batteries and supercapacitors. Furthermore, the dependence of current and charging timescales on a/λ is useful for the design of nanoporous electrodes. Our results are also informative for ion transport inside nanopores for biosensing and nanofluidic applications [38,39], and are especially relevant for ion transport in conical nanopores [40]. Our approach can be extended to account for finite ion size [41], dielectric decrement [42], electrolyte valence [43,44], electrolyte mixtures [45], asymmetric diffusivities [46] and atomistic physics [47,48]. Finally, our approach can also be extended to ion-selective electrodes and large potentials where additional effects such as concentration polarization can become important [49].

We thank the Andlinger Center for Energy and the Environment at Princeton University, and the National Science Foundation (CBET—1702693) for financial support. P. J. Z. would like to acknowledge ITHACA Project No. PPI/APM/2018/1/00045 financed by the Polish National Agency for Academic Exchange. The authors acknowledge that the work reported on in this Letter was performed using the Princeton Research Computing resources at Princeton University which is consortium of groups including the Princeton Institute for Computational Science and Engineering and the Princeton University Office of Information Technology's Research Computing department.

A. G. and P. J. Z. contributed equally to this work.

*hastone@princeton.edu

†ankur@princeton.edu

‡pjzuk@ippt.pan.pl

- [1] P. Simon and Y. Gogotsi, Materials for electrochemical capacitors, *Nat. Mater.* **7**, 845 (2008).
- [2] V. Presser, C. R. Dennison, J. Campos, K. W. Knehr, E. C. Kumbur, and Y. Gogotsi, The electrochemical flow capacitor: A new concept for rapid energy storage and recovery, *Adv. Energy Mater.* **2**, 895 (2012).

- [3] J. Newman and K. E. Thomas-Alyea, *Electrochemical Systems* (John Wiley & Sons, New York, 2012).
- [4] P. M. Biesheuvel, Y. Fu, and M. Z. Bazant, Diffuse charge and faradaic reactions in porous electrodes, *Phys. Rev. E* **83**, 061507 (2011).
- [5] P. M. Biesheuvel and M. Bazant, Nonlinear dynamics of capacitive charging and desalination by porous electrodes, *Phys. Rev. E* **81**, 031502 (2010).
- [6] P. Takhistov, Electrochemical synthesis and impedance characterization of nano-patterned biosensor substrate, *Biosens. Bioelectron.* **19**, 1445 (2004).
- [7] R. de Levie, On porous electrodes in electrolyte solutions: I. Capacitance effects, *Electrochim. Acta* **8**, 751 (1963).
- [8] H. A. Andreas, Self-discharge in electrochemical capacitors: a perspective article, *J. Electrochem. Soc.* **162**, A5047 (2015).
- [9] M. Kaus, J. Kowal, and D. U. Sauer, Modelling the effects of charge redistribution during self-discharge of supercapacitors, *Electrochim. Acta* **55**, 7516 (2010).
- [10] J. Kowal, E. Avaroglu, F. Chamekh, A. Šenfelds, T. Thien, D. Wijaya, and D. U. Sauer, Detailed analysis of the self-discharge of supercapacitors, *J. Power Sources* **196**, 573 (2011).
- [11] J. M. Black and H. A. Andreas, Pore shape affects spontaneous charge redistribution in small pores, *J. Phys. Chem. C* **114**, 12030 (2010).
- [12] J. W. Graydon, M. Panjehshahi, and D. W. Kirk, Charge redistribution and ionic mobility in the micropores of supercapacitors, *J. Power Sources* **245**, 822 (2014).
- [13] J. Huang, B. G. Sumpter, and V. Meunier, A universal model for nanoporous carbon supercapacitors applicable to diverse pore regimes, carbon materials, and electrolytes, *Chem. Eur. J.* **14**, 6614 (2008).
- [14] J. Huang, B. G. Sumpter, and V. Meunier, Theoretical model for nanoporous carbon supercapacitors, *Angew. Chem., Int. Ed. Engl.* **47**, 520 (2008).
- [15] M. Kroupa, G. J. Offer, and J. Kosek, Modelling of supercapacitors: Factors influencing performance, *J. Electrochem. Soc.* **163**, A2475 (2016).
- [16] C. Largeot, C. Portet, J. Chmiola, P.-L. Taberna, Y. Gogotsi, and P. Simon, Relation between the ion size and pore size for an electric double-layer capacitor, *J. Am. Chem. Soc.* **130**, 2730 (2008).
- [17] M. W. Verbrugge and P. Liu, Microstructural analysis and mathematical modeling of electric double-layer supercapacitors, *J. Electrochem. Soc.* **152**, D79 (2005).
- [18] M. Yaniv and A. Soffer, The transient behavior of an ideally polarized porous carbon electrode at constant charging current, *J. Electrochem. Soc.* **123**, 506 (1976).
- [19] W. G. Pell and B. E. Conway, Voltammetry at a de levie brush electrode as a model for electrochemical supercapacitor behaviour, *J. Electroanal. Chem.* **500**, 121 (2001).
- [20] W. Pell, B. Conway, and N. Marincic, Analysis of non-uniform charge/discharge and rate effects in porous carbon capacitors containing sub-optimal electrolyte concentrations, *J. Electroanal. Chem.* **491**, 9 (2000).
- [21] B. Conway and W. Pell, Power limitations of supercapacitor operation associated with resistance and capacitance distribution in porous electrode devices, *J. Power Sources* **105**, 169 (2002).

- [22] G. Madabattula and S. Kumar, Insights into charge-redistribution in double layer capacitors, *J. Electrochem. Soc.* **165**, A636 (2018).
- [23] H. Wang, J. Fang, and L. Pilon, Scaling laws for carbon-based electric double layer capacitors, *Electrochim. Acta* **109**, 316 (2013).
- [24] H. Wang and L. Pilon, Physical interpretation of cyclic voltammetry for measuring electric double layer capacitances, *Electrochim. Acta* **64**, 130 (2012).
- [25] L. Pilon, H. Wang, and A. d'Entremont, Recent advances in continuum modeling of interfacial and transport phenomena in electric double layer capacitors, *J. Electrochem. Soc.* **162**, A5158 (2015).
- [26] C. Lian, M. Janssen, H. Liu, and R. van Roij, Blessing and curse: How a supercapacitors large capacitance causes its slow charging, *Phys. Rev. Lett.* **124**, 076001 (2020).
- [27] M. A. Gebbie, M. Valtiner, X. Banquy, E. T. Fox, W. A. Henderson, and J. N. Israelachvili, Ionic liquids behave as dilute electrolyte solutions, *Proc. Natl. Acad. Sci. U.S.A.* **110**, 9674 (2013).
- [28] N. Gavish, D. Elad, and A. Yochelis, From solvent-free to dilute electrolytes: Essential components for a continuum theory, *J. Phys. Chem. Lett.* **9**, 36 (2018).
- [29] A. A. Lee, C. S. Perez-Martinez, A. M. Smith, and S. Perkin, Scaling Analysis of the Screening Length in Concentrated Electrolytes, *Phys. Rev. Lett.* **119**, 026002 (2017).
- [30] J. M. Huyghe and J. Janssen, Quadriphasic mechanics of swelling incompressible porous media, *Int. J. Eng. Sci.* **35**, 793 (1997).
- [31] See the Supplemental Material at <http://link.aps.org/supplemental/10.1103/PhysRevLett.125.076001> for the detailed description of experimental, theoretical and numerical methods, which includes Refs. [32–36].
- [32] H. G. Weller, G. Tabor, H. Jasak, and C. Fureby, A tensorial approach to computational continuum mechanics using object-oriented techniques, *J. Comput. Phys.* **12**, 620 (1998).
- [33] H. Jasak, A. Jemcov, and Z. Tukovic, OpenFOAM: A C++ library for complex physics simulations, in *International Workshop on Coupled Methods in Numerical Dynamics* (IUC Dubrovnik, Croatia, 2007), Vol. 1000, pp. 1–20.
- [34] R. Eymard, T. Gallouët, and R. Herbin, Finite volume methods, *Handbook Numer. Anal.* **7**, 713 (2000).
- [35] H. K. Versteeg and W. Malalasekera, *An Introduction to Computational Fluid Dynamics: The Finite Volume Method* (Pearson Education, 2007), http://ftp.demec.ufpr.br/disciplinas/TM702/Versteeg_Malalasekera_2ed.pdf.
- [36] R. I. Issa, Solution of the implicitly discretised fluid flow equations by operator-splitting, *J. Comput. Phys.* **62**, 40 (1986).
- [37] R. Tivony, S. Safran, P. Pincus, G. Silbert, and J. Klein, Charging dynamics of an individual nanopore, *Nat. Commun.* **9**, 1 (2018).
- [38] S. Faucher, N. Aluru, M. Z. Bazant, D. Blankschtein, A. H. Brozena, J. Cumings, J. Pedro de Souza, M. Elimelech, R. Epsztein, J. T. Fourkas *et al.*, Critical knowledge gaps in mass transport through single-digit nanopores: A review and perspective, *J. Phys. Chem. C* **123**, 21309 (2019).
- [39] R. B. Schoch, J. Han, and P. Renaud, Transport phenomena in nanofluidics, *Rev. Mod. Phys.* **80**, 839 (2008).
- [40] J. Cervera, B. Schiedt, and P. Ramirez, A poisson/nernst-planck model for ionic transport through synthetic conical nanopores, *Europhys. Lett.* **71**, 35 (2005).
- [41] D. Gillespie, A review of steric interactions of ions: Why some theories succeed and others fail to account for ion size, *Microfluid. Nanofluid.* **18**, 717 (2015).
- [42] Y. Nakayama and D. Andelman, Differential capacitance of the electric double layer: The interplay between ion finite size and dielectric decrement, *J. Chem. Phys.* **142**, 044706 (2015).
- [43] A. Gupta and H. A. Stone, Electrical double layers: effects of asymmetry in electrolyte valence on steric effects, dielectric decrement, and ion–ion correlations, *Langmuir* **34**, 11971 (2018).
- [44] A. Gupta, B. Rallabandi, and H. A. Stone, Diffusiophoretic and diffusioosmotic velocities for mixtures of valence-asymmetric electrolytes, *Phys. Rev. Fluids* **4**, 043702 (2019).
- [45] A. Gupta, S. Shim, L. Issah, C. McKenzie, and H. A. Stone, Diffusion of multiple electrolytes cannot be treated independently: model predictions with experimental validation, *Soft Matter* **15**, 9965 (2019).
- [46] S. H. Amrei, S. C. Bukosky, S. P. Rader, W. D. Ristenpart, and G. H. Miller, Oscillating Electric Fields in Liquids Create a Long-Range Steady Field, *Phys. Rev. Lett.* **121**, 185504 (2018).
- [47] D. Jiang, Z. Jin, and J. Wu, Oscillation of capacitance inside nanopores, *Nano Lett.* **11**, 5373 (2011).
- [48] G. Feng and P. T. Cummings, Supercapacitor capacitance exhibits oscillatory behavior as a function of nanopore size, *J. Phys. Chem. Lett.* **2**, 2859 (2011).
- [49] I. Rubinstein and B. Zaltzman, Dynamics of extended space charge in concentration polarization, *Phys. Rev. E* **81**, 061502 (2010).